

Revisiting The Mass-Size Relation Of Structures In Molecular Clouds

Yuchen Xing^{1,2} and Keping Qiu^{1,2}

¹ School of Astronomy and Space Science, Nanjing University, Nanjing 210023, P. R. China;
kpqiu@nju.edu.cn

² Key Laboratory of Modern Astronomy and Astrophysics (Nanjing University), Ministry of Education, Nanjing 210023, P.R.China

Received 20xx month day; accepted 20xx month day

Abstract We revisit the mass-size relation of molecular cloud structures based on the column density map of the Cygnus-X molecular cloud complex. We extract 135 column density peaks in Cygnus-X and analyze the column density distributions around these peaks. The averaged column density profiles, $N(R)$, around all the peaks can be well fitted with broken power-laws, which are described by an inner power-law index n , outer power-law index m , and the radius R_{TP} and column density N_{TP} at the transition point. We then explore the $M - R$ relation with different samples of cloud structures by varying the $N(R)$ parameters and the column density threshold, N_0 , which determines the boundary of a cloud structure. We find that only when N_0 has a wide range of values, the $M - R$ relation may largely probe the density distribution, and the fitted power-law index of the $M - R$ relation is related to the power-law index of $N(R)$. On the contrary, with a constant N_0 , the $M - R$ relation has no direct connection with the density distribution; in this case, the fitted power-law index of the $M - R$ relation is equal to 2 (when $N_0 \geq N_{\text{TP}}$ and n has a narrow range of values), larger than 2 (when $N_0 \geq N_{\text{TP}}$ and n has a wide range of values), or slightly less than 2 (when $N_0 < N_{\text{TP}}$).

Key words: methods: analytical — methods: data analysis — ISM: clouds — ISM: structure

1 INTRODUCTION

The density distribution reflects the physical state of a molecular cloud thus is important for understanding star formation. However, both volume and column density distributions are difficult to obtain in large quantities directly. Dust extinctions in optical and near-infrared bands can be used to derive H_2 distribution at high resolution but cannot probe dense regions (Lada et al. 1994; Lombardi & Alves 2001). Although dust continuum and molecular lines at millimeter and sub-millimeter wavelengths are free of this problem, they are limited by the low resolution of single-dish radio telescopes and the small dynamic range of interferometers (Kellermann & Moran 2001). Moreover, obtaining the density distributions of a large number of sources across orders of magnitude in density and size is always time-consuming regardless of the observation method used. For decades, the mass-size relation between different structures (hereafter, the $M - R$ relation) has been an important way to explore the density distribution of molecular gas.

An early result of the $M - R$ relation comes from Larson (1981). Their famous Larson Third law indicated that the density – size relation at $0.1 - 100\text{pc}$ is $n(\text{H}_2) \propto L^{-1.10}$, corresponding to $M \propto R^{1.9}$.

The relation was considered to represent a density distribution of $\rho \propto R^{-1}$, implying that the structures they used in obtaining the $M - R$ relation have approximately the same averaged column density. Since then, there have been a number of observational studies deriving a variety of $M - R$ relations from $M \propto R^{1.4}$ to $M \propto R^{3.0}$, which have been interpreted as $\rho \propto R^{-\alpha}$ distributions with $\alpha = 0 - 1.6$. The $M \propto R^2$ relation is the most commonly seen relation and has been observed in all scales from 10^{-2} pc to 10^2 pc (Larson 1981; Schneider & Brooks 2004; Lada & Dame 2020; Mannfors et al. 2021), while the other indexes are mainly observed at $10^{-2} - 10^1$ pc (Roman-Duval et al. 2010; Urquhart et al. 2018; Traficante et al. 2018; Massi et al. 2019; Lin et al. 2019).

However, how reliable or accurate the $M - R$ relations are probing the density distributions is still a matter of debate. Observational biases, including the sensitivity limit (Kegel 1989; Schneider & Brooks 2004) and the column density selection effects for certain tracers (Scalo 1990; Ballesteros-Paredes & Mac Low 2002), as well as the source extraction methodologies (Kegel 1989; Schneider & Brooks 2004; Heyer et al. 2009), can all play a role in the derived $M - R$ relations, and thus affect the inferred density distributions. In the 2000s, dust continuum surveys brought new opportunities to understand the $M - R$ relation (Enoch et al. 2006; Pirogov et al. 2007). The advent of the Herschel observatory (Pilbratt et al. 2010) made it possible to map simultaneously extended and compact dust continuum emissions at multi-wavelengths in the far-infrared to sub-millimeter window. Consequently, the column density profiles (hereafter, $N(R)$ profiles) of dense molecular cloud structures can be derived at moderate angular resolutions (Arzoumanian et al. 2011; Kauffmann et al. 2010; Schneider et al. 2013). The $N(R)$ profiles are found to have different indexes at different scales and their corresponding $M(R)$ profiles may be inconsistent with the $M - R$ relation (Pirogov 2009; Lombardi et al. 2010; Kauffmann et al. 2010; Beaumont et al. 2012). Lombardi et al. (2010), Beaumont et al. (2012), and Ballesteros-Paredes et al. (2012) pointed out that measuring the $M - R$ relations based on observations in general implies an effective column density threshold, which in turn would naturally lead to a $M \propto R^2$ relation for typical column density probability distribution functions (N-PDFs), such as log-normal (Lombardi et al. 2010; Beaumont et al. 2012), power-law (Ballesteros-Paredes et al. 2012) or log-normal + power-law (Ballesteros-Paredes et al. 2012) N-PDFs. However, there has been no study that links real observational $M(R)$ profiles with $M - R$ relations through mathematical calculations.

In this paper, using the Cygnus-X column density map from Cao et al. (2019), we obtain $N(R)$ profiles of 135 dense structures at $0.1 - 10$ pc. It enables us to derive $M - R$ relations from real density profiles, thus deepening the understanding of the $M - R$ relations, density distributions, and the physical states behind them. We present the obtained $N(R)$ profiles and their parameter distributions in Section 2. In Section 3, we study effects of the $N(R)$ profiles and column density threshold N_0 on the $M - R$ relation. We further discuss the significance of the $N(R)$ profile and the $M - R$ relation from a more realistic perspective in Section 4. The results are summarized in Section 5.

2 $N(R)$ PROFILES OF CYGNUS-X

Cygnus-X is one of the most massive giant molecular clouds in our Galaxy (Motte et al. 2018), and shows rich star formation activities evidenced by numerous HII regions, OB associations, dense molecular gas clumps and cores (Wendker et al. 1991; Uyaniker et al. 2001; Motte et al. 2007; Cao et al. 2019; Wang et al. 2022). It is located at a distance of 1.4 kpc from the Sun (Rygl et al. 2012). Using *getsources* (Men'Shchikov et al. 2012), Cao et al. (2019) applied SED fittings to the 160, 250, 350, and 500 μm dust continuum images from *Herschel*, and obtained the temperature map and the column density map of Cygnus-X. The resolution of the column density map was set by the SED fitting of the smallest spatial scale component using the 160 and 250 μm data, and is $18.''4$ determined by the 250 μm images, corresponding to 0.1 pc at the distance of 1.4 kpc. Using the column density map, Xing et al. (in preparation) obtained the N-PDF of the complex, which shows a log-normal + power-law shape. The turbulence-dominated log-normal component and the gravity-dominated power-law component are delimited by a transitional column density at $1.86 \times 10^{22} \text{cm}^{-2}$ (Xing et al. in preparation). We selected all column density peaks above $1.86 \times 10^{22} \text{cm}^{-2}$ for the extraction of density profiles. To avoid the influence of structures that cannot be described by radial density profiles, we check the morphology of

every structure within a density threshold of $1.86 \times 10^{22} \text{cm}^{-2}$, and exclude those with aspect ratios larger than 2. In this way, we eventually obtained 135 peaks which are shown in Figure 1. We divide the area around each column density peak into 24 sectors with the same angular size (i.e., 15 degrees). For each sector, we calculate the distance of each pixel to the column density peak and average all pixels with the same distance to obtain a sectorized radial $N(R)$ profile. Thus for each column density peak we have 24 $N(R)$ profiles extracted from 10 pc down to the resolution at 0.1 pc. We then discard any sectorized profiles that show a column density rise of more than $6.46 \times 10^{21} \text{cm}^{-2}$, which is the peaking column density of the log-normal part in Cygnus-X's N-PDF, with the increasing radius to bypass the contamination from nearby sources. We average the remaining sectorized $N(R)$ profiles to obtain a final $N(R)$ profile for each column density peak. The obtained $N(R)$ profiles are shown in Figure 2. In the sections below, to distinguish from the structures used in the $M - R$ relation, we call these 135 structures extending outward from the column density peaks to about 10 pc the 135 Cygnus-X clumps. Note that they are not ‘clumps’ in the usual definition, and have no strict boundaries.

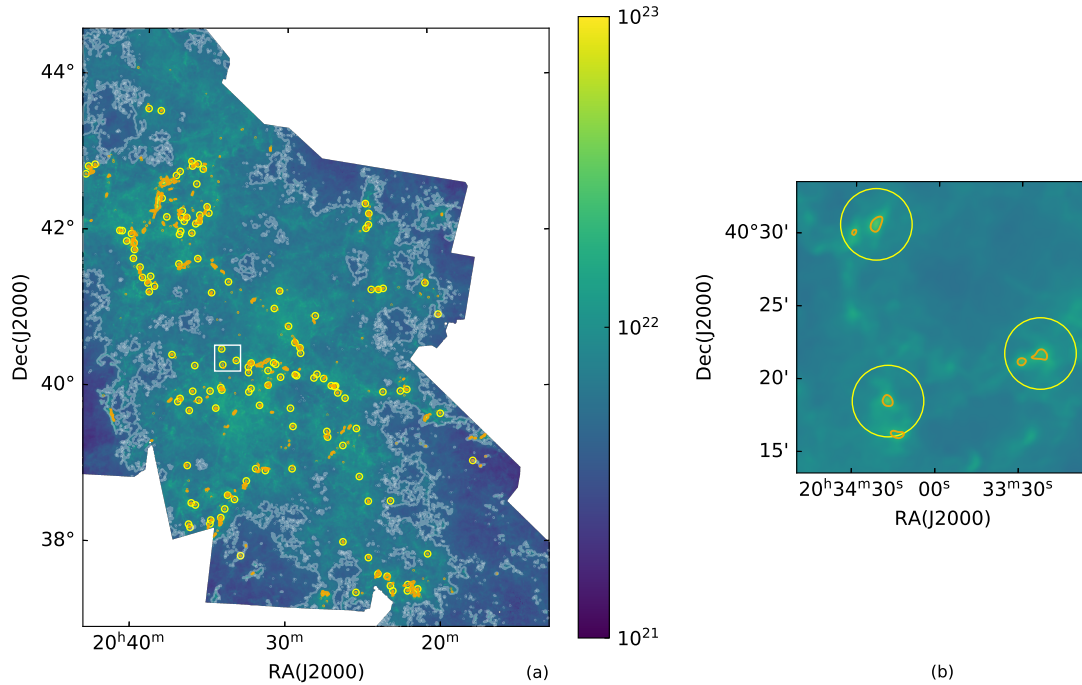


Fig. 1: The column density map of Cygnus-X in $[\text{cm}^{-2}]$. *a)* Yellow circles denote the 1 pc radius around the 135 peaks. White contours outline the regions with column densities higher than $5.0 \times 10^{21} \text{cm}^{-2}$. Orange contours outline the regions with column densities higher than $1.86 \times 10^{22} \text{cm}^{-2}$. *b)* A zoom-in image of the area outlined by the white rectangle in panel (*a*), to better display the morphology of the column density distribution around the selected density peaks.

The $N(R)$ profiles are apparently steep in the inner part and flat in the outer part, with the break points roughly around 1 pc (see Figure 2). We then fit the $N(R)$ profiles with a broken power-law distribution as described by

$$N = \begin{cases} N_{\text{TP}} \left(\frac{R}{R_{\text{TP}}} \right)^{-n} & R \leq R_{\text{TP}} \\ N_{\text{TP}} \left(\frac{R}{R_{\text{TP}}} \right)^{-m} & R > R_{\text{TP}} \end{cases} \quad (1)$$

where n is the power-law index of the inner region, m the power-law index of the outer region, and N_{TP} and R_{TP} are the transitional column density and radius at the break point, respectively. We obtain good

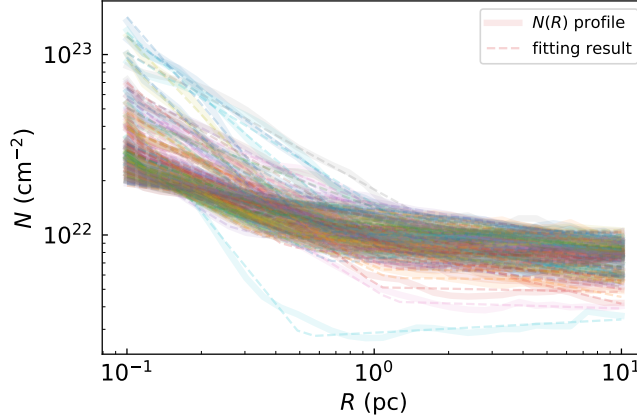


Fig. 2: Radial $N(R)$ profiles of the 135 clumps at $R = 0.1 - 10$ pc. The corresponding broken power-law fittings are shown in dashed lines.

fittings for all the 135 clumps with R -squared values all above 0.93. Figure 3 shows the histograms of the four $N(R)$ parameters of the fitting result.¹ 95% of the clumps have power-law index $n = 0.63 \pm 0.59$ at radius $R \leq R_{\text{TP}}$, corresponding to $M(R) \propto R^{1.37 \pm 0.59}$ and $\rho \propto R^{-(1.63 \pm 0.59)}$ assuming spherical symmetry. These profiles are close to the free-fall collapse which has $\rho \propto R^{-\alpha}$ with $\alpha = 1.5 - 2.0$, suggesting their gravity-dominated nature. 20 clumps have n larger than 1. The largest n goes up to 1.69, corresponding to a steep density profile with $\alpha = 2.69$, which is far beyond the free-fall collapse. At $R > R_{\text{TP}}$, the clumps have similar column densities. The outer $N(R)$ index m has a tight distribution, with a 95% distribution interval of $m = 0.11 \pm 0.20$. It corresponds $M(R) \propto R^{1.89 \pm 0.20}$ and $\rho \propto R^{-(1.11 \pm 0.20)}$, suggesting the turbulence-dominated nature. R_{TP} and N_{TP} have 95% distribution intervals of $R_{\text{TP}} = 0.78^{+2.69}_{-0.60}$ pc and $N_{\text{TP}} = 1.00^{+0.70}_{-0.41} \times 10^{22} \text{ cm}^{-2}$, respectively. These values, of approximately $R = 1$ pc and $N = 10^{22} \text{ cm}^{-2}$, mark the transition between the two components.

3 FROM $N(R)$ PROFILES TO $M - R$ RELATIONS

3.1 Obtaining the $M - R$ relation

By integrating the broken power-law $N(R)$ profile, we can obtain the $M(R)$ profile as

$$M = 2\pi M_{\text{H}_2} \times \begin{cases} \frac{1}{2-n} \frac{N_{\text{TP}}}{R_{\text{TP}}^n} R^{2-n} & R \leq R_{\text{TP}} \\ \frac{1}{2-n} N_{\text{TP}} R_{\text{TP}}^2 + \frac{1}{2-m} \frac{N_{\text{TP}}}{R_{\text{TP}}^m} (R - R_{\text{TP}})^{2-m} & R > R_{\text{TP}}, \end{cases} \quad (2)$$

where $M_{\text{H}_2} = 3.32 \times 10^{-24} \text{ g}$ is the hydrogen molecule mass. It is clear that, the $M(R)$ profile has a shape close to broken power-law and is fully described by the four $N(R)$ parameters.

The well known $M - R$ relation is obtained by intercepting a group of $M(R)$ profiles with some column density threshold N_0 . In real observations, N_0 is determined by either observational limits, such as the detection limit which is typically a few times the noise level, or by the selection effect of a source extraction algorithm (e.g., Kegel 1989; Scalo 1990; Ballesteros-Paredes & Mac Low 2002). With the column density threshold N_0 determined, the mass M and radius R in a $M - R$ relation are defined as

$$M = 2\pi M_{\text{H}_2} \times \begin{cases} \frac{N_{\text{TP}}^{2/n} R_{\text{TP}}^2}{2-n} N_0^{1-\frac{2}{n}} & N_0 \geq N_{\text{TP}} \\ \left(\frac{1}{2-n} - \frac{1}{2-m} \right) N_{\text{TP}} R_{\text{TP}}^2 + \frac{N_{\text{TP}}^{2/m} R_{\text{TP}}^2}{2-m} N_0^{1-\frac{2}{m}} & N_0 < N_{\text{TP}} \end{cases} \quad (3)$$

¹ Note that all radii we use refer to the full radii instead of half-widths at half maximums which are often used in core statistics.

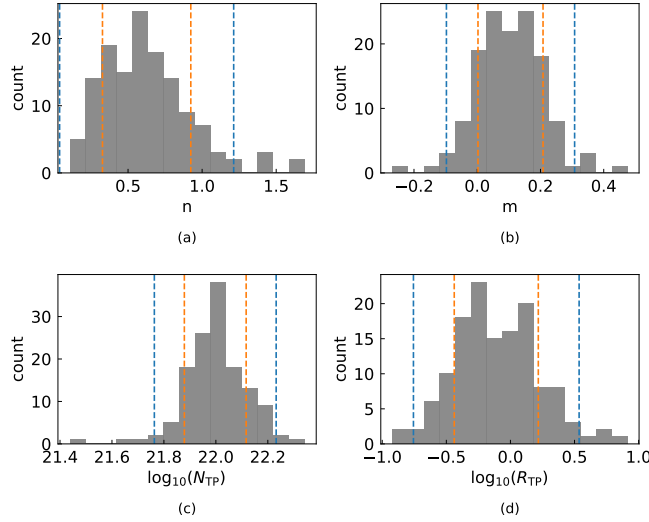


Fig. 3: Parameters derived by performing broken power-law fittings to the 135 Cygnus-X clumps. Orange and blue dashed lines show the 1σ (68%) and 2σ (95%) distribution intervals, respectively. *a)* The distribution of the inner power-law index n . *b)* The distribution of the outer power-law index m . *c)* The distribution of the transitional column density N_{TP} . *d)* The distribution of R_{TP} , the radius at the transitional point.

and

$$R = \begin{cases} R_{\text{TP}} \left(\frac{N_0}{N_{\text{TP}}} \right)^{-1/n} & N_0 \geq N_{\text{TP}} \\ R_{\text{TP}} \left(\frac{N_0}{N_{\text{TP}}} \right)^{-1/m} & N_0 < N_{\text{TP}}. \end{cases} \quad (4)$$

Thus the mass and radius of a structure in a $M - R$ relation are determined by both the four $N(R)$ parameters and the column density threshold N_0 . Further, combining Equation 3 and Equation 4, the $M - R$ relation can be given by

$$M = 2\pi M_{\text{H}_2} \times \begin{cases} \frac{N_0}{2-n} R^2 & N_0 \geq N_{\text{TP}} \\ \left(\frac{1}{2-n} - \frac{1}{2-m} \right) N_{\text{TP}} R_{\text{TP}}^2 + \frac{N_0}{2-m} R^2 & N_0 < N_{\text{TP}}. \end{cases} \quad (5)$$

From Equation 5, the $M - R$ relation at $N_0 \geq N_{\text{TP}}$ is apparently a function of R^2 , and is simplified to $M \propto R^2$ if all the clumps have the same inner power-law index n and are trimmed at a constant N_0 . Otherwise, the $M - R$ relation deviates from $M \propto R^2$ at a degree depending both on the density profile $N(R)$ and the threshold density N_0 . We explore the $M - R$ relation in detail in the following subsection.

3.2 Effects of the $N(R)$ parameters and N_0

Here we study the effects of the density profile $N(R)$ and the column density threshold N_0 on the $M - R$ relation. For convenience, we start with $N_0 \geq N_{\text{TP}}$, and then extend the analysis to the $N_0 < N_{\text{TP}}$ regime.

First, assume that n and N_0 are constant. The case of single power-law density profiles with constant n and N_0 was analyzed in Ballesteros-Paredes et al. (2012). It is easy to see from Equation 5 that the corresponding $M - R$ relation will show a perfect $M \propto R^2$ shape. Figure 4 shows an example of this circumstance. All the 50 $M(R)$ profiles in the figure have $n = 0.63$ and $m = 0.11$. We assume that the N_{TP} and R_{TP} values have Gaussian distributions. We use $\sigma_{NR_{\text{TP}}}$ to describe the Gaussian

distributions of N_{TP} and R_{TP} with average values of 10^{22}cm^{-2} and 0.78pc . And the $\mu \pm \sigma$ ranges of N_{TP} and R_{TP} are given by $10^{22.00 \pm 0.12 \sigma_{NR_{\text{TP}}}}\text{cm}^{-2}$ and $10^{-0.11 \pm 0.33 \sigma_{NR_{\text{TP}}}}\text{pc}$ (where μ and σ are the mean and standard deviation of a Gaussian distribution). $\sigma_{NR_{\text{TP}}} = 1$ is used in Figure 4. We adopt $N_0 = 2.5 \times 10^{22}\text{cm}^{-2}$ and obtain a sample of structures. We then fit the $M - R$ relation with a power-law model. Only structures within $0.1 - 10\text{pc}$ are included in the fitting. The fitting result indeed shows a perfect $M \propto R^2$ relation, which is consistent with the analysis of Ballesteros-Paredes et al. (2012) and the calculations above. For comparison, we lower N_0 to $8.0 \times 10^{21}\text{cm}^{-2}$, a value slightly below N_{TP} , and find that the $M - R$ relation follows $M \propto R^{1.90}$, which is very close to the $M \propto R^2$ relation.

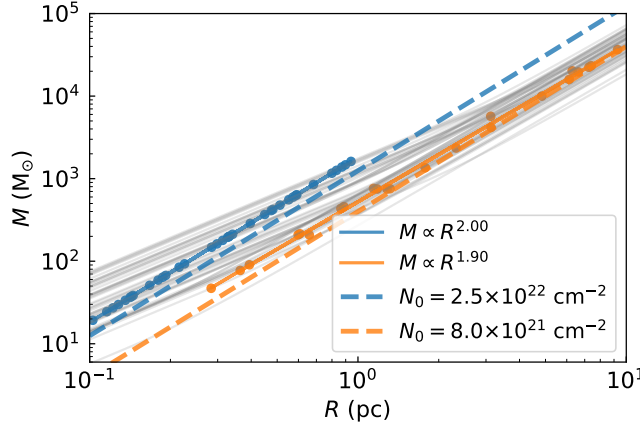


Fig. 4: Gray lines show a set of $M(R)$ profiles equivalent to column density profiles that have $n = 0.63$, $m = 0.11$, and $\sigma_{NR_{\text{TP}}} = 1$. Blue and orange dots mark the data points obtained by intercepting those $M(R)$ profiles with $N_0 = 2.5 \times 10^{22}\text{cm}^{-2}$ and $N_0 = 8.0 \times 10^{21}\text{cm}^{-2}$, respectively. The data points are used to fit the $M - R$ relations (solid lines). Blue and orange dashed lines indicate $M(R)$ profiles corresponding to constant column densities of $2.5 \times 10^{22}\text{cm}^{-2}$ and $8.0 \times 10^{21}\text{cm}^{-2}$, respectively.

We then study the effects of the $N(R)$ index on the $M - R$ relation, i.e., effects of n when $N_0 \geq N_{\text{TP}}$. We generate 20 density profiles with $m = 0.11$ and $\sigma_{NR_{\text{TP}}} = 0$. Their n values are evenly distributed in the range of $0 - 1.2$. In Figure 5, these density profiles correspond to $M(R)$ profiles that are almost the same at larger radii and have different indexes at smaller radii. $M(R)$ profiles with larger n have shallower indexes at $R \leq R_{\text{TP}}$. As in Equation 5, for any n between 0 and 2 (Note that n cannot be equal to 2 in order to obtain a finite mass. n with a value outside the range of $0 - 2$ is impractical for it will either correspond to a $N(R)$ profile that is denser on the larger radii, or have a density profile steeper than $\rho \propto R^{-3}$), M always increases with n . When adopting $N_0 = 2.5 \times 10^{22}\text{cm}^{-2}$, from bottom to top, the n value increases and the data points deviate more from the $M \propto R^2$ line. The $M - R$ relation is apparently steeper than $M \propto R^2$ and bends upward at the high mass end. While for the case with $N_0 = 5.0 \times 10^{22}\text{cm}^{-2}$, only 7 structures with the largest n fall in $0.1 - 10\text{pc}$. It makes the n range of the used data smaller, so the bending is less obvious. But the $M - R$ relation is still steeper than $M \propto R^2$.

In Figure 6 we show the effect of N_{TP} and R_{TP} on the $M - R$ relation. As in the $N_0 > N_{\text{TP}}$ part of Equation 3 and Equation 4, both M and R^2 are proportional to $N_{\text{TP}}^{2/n} R_{\text{TP}}^2$. Therefore, N_{TP} or R_{TP} with wider ranges will make the data points distribute within a larger range along the $M \propto R^2$ line. It will eventually make the $M - R$ index approaches 2, regardless of the original value of the $M - R$ index. The density profiles in panel (a) of Figure 6 have n and m generated in the same way as those in Figure 5, but their N_{TP} and R_{TP} follow $\sigma_{NR_{\text{TP}}} = 0.5$. Adopting $N_0 = 2.5 \times 10^{22}\text{cm}^{-2}$ and $5.0 \times 10^{22}\text{cm}^{-2}$, the $M - R$ relations are found to be closer to $M \propto R^2$ compared to their counterparts in Figure 5. With N_{TP} and R_{TP} varying over a large range, the bendings caused by n are washed out. We then fit the two $M - R$ relations with power-law models and the results are $M \propto R^{2.29}$ and $M \propto R^{2.18}$. We further

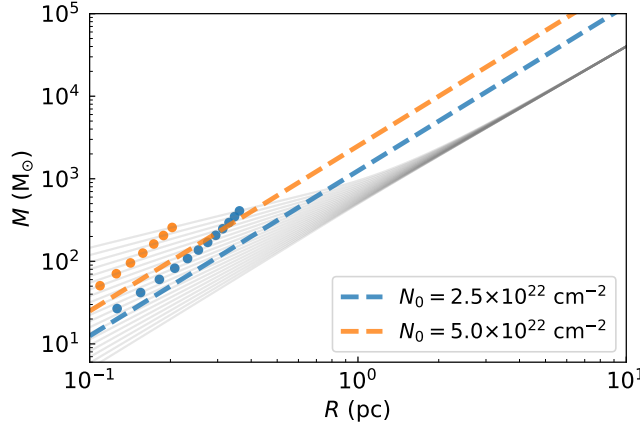


Fig. 5: Same as Figure 4, but for $m = 0.11$, $\sigma_{NR_{TP}} = 0$, n evenly distributed from 0 to 1.2, and $N_0 = 2.5 \times 10^{22} \text{ cm}^{-2}$ and $N_0 = 5.0 \times 10^{22} \text{ cm}^{-2}$.

increase the Gaussian distributions of N_{TP} and R_{TP} to $\sigma_{NR_{TP}} = 1$ in panel (b) of Figure 6. The fitting results of the $M - R$ relation are $M \propto R^{2.18}$ and $M \propto R^{2.11}$, which are closer to $M \propto R^2$ compared to those in panel (a).

Figure 7 shows the effects of N_0 on the $M - R$ relation. In panel (a) of Figure 7, we adopt $n = 0.63$, $m = 0.11$, and $\sigma_{NR_{TP}} = 1$. Note that the corresponding $M - R$ relation will inevitably be affected by the wide N_{TP} and R_{TP} ranges as discussed above. The n value corresponds to $M(R) \propto R^{1.37}$ at $N \geq N_{TP}$. According to Equation 5, $\frac{M}{R^2}$ is proportional to N_0 , meaning that the variation in N_0 would wash out the $M \propto R^2$ relation. In addition, considering an extreme that the clumps under investigation all have an identical density profile, differing N_0 is to catch structures falling on different positions along the $M(R)$ profile, and the $M - R$ relation would have a shape the same as that of the $M(R)$ profile provided the sample is large enough and N_0 is randomly drawn from a wide range. We adopt $N_0 = (0.1 - 2.5) \times 10^{23} \text{ cm}^{-2}$. The N_0 range covers the column densities of most $M(R)$ profiles at $N \geq N_{TP}$, but it also includes some $M(R)$ profiles at $N < N_{TP}$. For simplicity, we only use data points with $N \geq N_{TP}$ for fitting and obtain $M \propto R^{1.50}$. This can be understood as a combined effect of varying N_{TP} , R_{TP} , and the large range of N_0 , with the former having a tendency of $M \propto R^2$ and the latter getting the $M - R$ relation close to the $M(R)$ profile. In panel (b) of Figure 7, we change n to have a Gaussian distribution with the $\mu \pm \sigma = 0.63 \pm 0.30$. The obtained $M - R$ index does not change since the averaged value of n is still 0.63. It is also noticeable that allowing N_0 to vary within a range will induce significant scatter of the data points in the $M - R$ plot.

Let's then consider the $N < N_{TP}$ part of the $M - R$ relation. Firstly, the $\frac{N_0}{2-m} R^2$ term of the $N < N_{TP}$ part is similar to the $M - R$ relation at $N \geq N_{TP}$ (see Equation 5), thus the $N < N_{TP}$ part has all the effects discussed above. Aside from these, the $N < N_{TP}$ part has an additional $\left(\frac{1}{2-n} - \frac{1}{2-m}\right) N_{TP} R_{TP}^2$ term. It represents the additional mass introduced by the $N \geq N_{TP}$ part and is independent of N_0 . Considering that n is larger than m , this term will increase the obtained mass. As in Equation 2, for any structure trimmed by a threshold with $N_0 < N_{TP}$, the smaller its radius, the larger the proportion of this term in the total mass. Therefore, the existence of this term will shift the left end of the $M - R$ relation more upward, and thus flatten the $M - R$ relation (e.g., $M \propto R^{1.90}$ in the case shown in orange in Figure 4).

Now we can summarize the effects of the $N(R)$ parameters and the column density threshold N_0 on the $M - R$ relation as follows: (1) constant $N(R)$ profile power-law index and constant N_0 give rise to a $M \propto R^2$ tendency; (2) the $N(R)$ power-law index with a wide range steepens the $M - R$ relation; (3) N_{TP} and R_{TP} with wide ranges to some extent weaken the steepening effect due to the variation of the $N(R)$ power-law index; (4) N_0 with a wide range tend to wash out the $M \propto R^2$ relation and get the

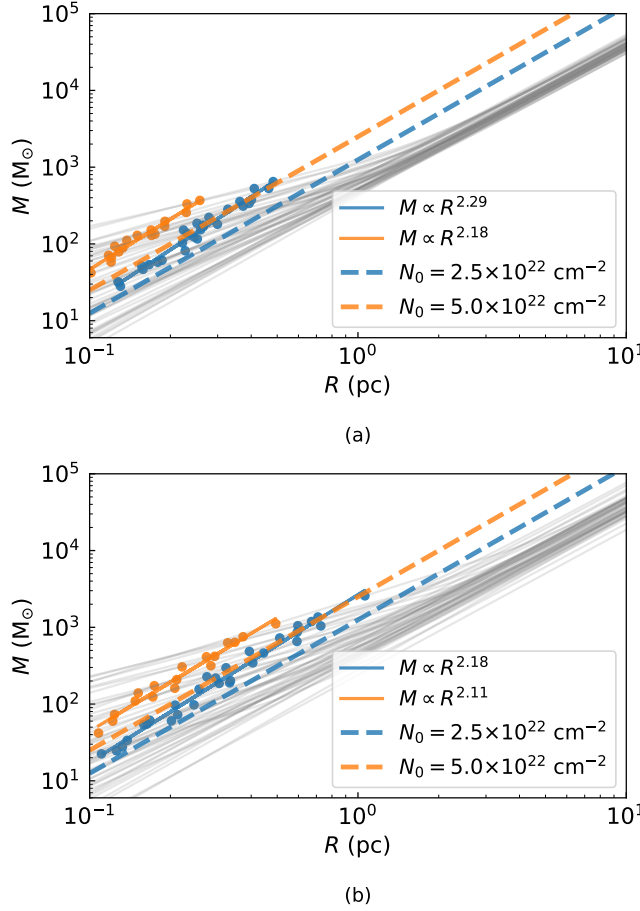


Fig. 6: Same as Figure 5, but for $\sigma_{NR_{TP}} = 0.5$ in panel (a) and $\sigma_{NR_{TP}} = 1.0$ in panel (b).

$M - R$ relation approaching the averaged density profile of the sample sources; (5) at $N < N_{TP}$, the fact that n is larger than m makes the $M - R$ index lower than 2.

3.3 The $M - R$ relation of the 135 Cygnus-X clumps

Using the 135 Cygnus-X clumps, we look into the $M - R$ relations from a more realistic perspective. The $N(R)$ parameters of the 135 clumps are described in Section 2. By fixing N_0 at a certain value, or allowing it to vary within a range, we obtain six samples of the clumps. We then fit the $M - R$ relations with power-law models. Only structures within $0.1 - 10$ pc are included in the fitting. The results are shown in Figure 8.

Cases 1-3 have their N_0 fixed at a certain value. We adopt $N_0 = 7.9 \times 10^{21} \text{ cm}^{-2}$ in Case 1. This N_0 is lower than N_{TP} of most clumps, and the obtained structures mainly fall at $1 - 10$ pc. The $M - R$ relation is similar to that shown in orange in Figure 4: the constant N_0 favors a $M \propto R^2$ relation, while $N_0 < N_{TP}$ makes the $M - R$ index slightly lower. The difference of m between the 135 clumps increases the $M - R$ index, but the increase is negligible since m has a narrow distribution. These all finally lead to a $M \propto R^{1.81}$ relation. In Case 2 and 3, We adopt $N_0 = 2.5 \times 10^{22} \text{ cm}^{-2}$ and $N_0 = 5.0 \times 10^{22} \text{ cm}^{-2}$. These N_0 are higher than all of the N_{TP} values of the 135 clumps, and the obtained structures all fall at $0.1 - 1$ pc. The $M - R$ relations are similar to those in Figure 5 and

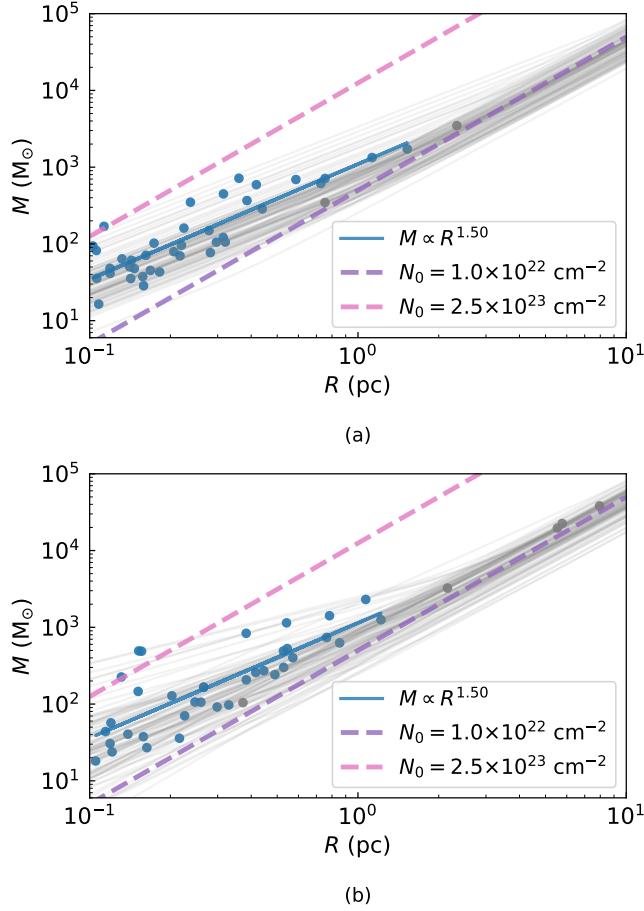


Fig. 7: *a*): Same as Figure 4, but for N_0 ranging from $1.0 \times 10^{22} \text{ cm}^{-2}$ to $2.5 \times 10^{23} \text{ cm}^{-2}$. The $M(R)$ profiles corresponding to the upper and lower limits of N_0 are shown in pink and purple dashed lines, respectively. Blue and gray points correspond to structures with $N_0 \geq N_{\text{TP}}$ and $N_0 < N_{\text{TP}}$, respectively. The fitting result of the blue points is shown in the solid blue line. *b*): same as panel (*a*), but for n having a Gaussian distribution with $\mu \pm \sigma = 0.63 \pm 0.30$, where μ and σ are the mean and standard deviation of the Gaussian distribution.

Figure 6: on top of the $M \propto R^2$ trend contributed by the constant N_0 , the difference between n makes the $M - R$ relations steeper, leading to $M \propto R^{2.22}$ and $M \propto R^{2.40}$.

In Cases 4-6, N_0 of each structure is randomly generated within a range in logarithmic space. Most structures obtained in Case 4 have radii falling in the range of 1–10 pc. The N_0 range of $10^{21.9 \pm 0.2} \text{ cm}^{-2}$ is wide enough to cover the column densities of most clumps below N_{TP} . With the wide N_0 range, the $M - R$ relation can potentially probe the density profiles in the $N < N_{\text{TP}}$ regime. However, there are still some structures with sizes of 0.1–1 pc, at which the $M(R)$ profiles have their mean as $M(R) \propto R^{1.37}$. These structures make the obtained $M - R$ relation slightly shallower than the mean $M(R)$ profile of $M(R) \propto R^{1.89}$ for $N < N_{\text{TP}}$, and the fitting result is $M \propto R^{1.75}$. In Case 5 we use $N_0 = 10^{22.4 \pm 0.7} \text{ cm}^{-2}$. The N_0 range covers the column densities of most clumps at 0.1–10 pc. In this case, both the 0.1–1 pc and 1–10 pc parts contain a considerable number of structures, and the $M - R$ index at 1.56 is also in the middle of the mean $M(R)$ profile indexes of the two parts. In Case 6 we adopt $N_0 = 10^{22.7 \pm 0.7} \text{ cm}^{-2}$. The N_0 range covers the column densities of most clumps at 0.1–1 pc.

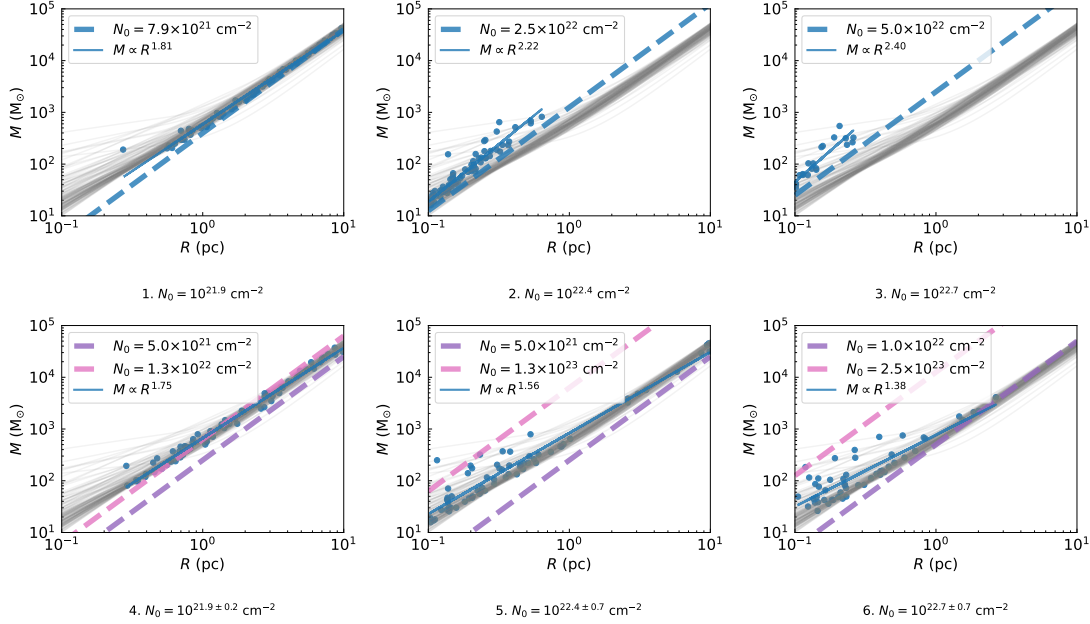


Fig. 8: $M - R$ relations derived from the $M(R)$ profiles of the 135 Cygnus-X clumps, which are intercepted with different choices of N_0 as indicated below each panel. Other symbols are the same as those shown in Figure 4-7.

Most of the obtained structures have sizes of $0.1 - 1$ pc, and the $M \propto R^{1.38}$ relation is very close to the mean $M(R)$ profile for $N \geq N_{\text{TP}}$.

We further obtain the $M - R$ indexes in Figure 9. By simply varying the mean and range of N_0 , $M - R$ relations with indexes from 1.4 to 2.4 are obtained from the 135 clumps. When N_0 is fixed at a certain value, we obtain $M - R$ relations with indexes of 1.8 – 2.4. The $M - R$ relations with $N_0 < 10^{22.1} \text{ cm}^{-2}$ have indexes around 1.8 – 1.9. At higher N_0 , we obtain $M - R$ relations with indexes of 2 – 2.4. When N_0 has a sufficiently wide range, the $M - R$ index is always smaller than 2 and decreases with the increase of N_0 . These indexes manifest the density profiles at the corresponding scales. The decreasing trend comes from the difference between the mean shapes of the two parts of the $M(R)$ profiles, i.e., $M(R) \propto R^{1.89}$ for $R > R_{\text{TP}}$ and $M(R) \propto R^{1.37}$ for $R \leq R_{\text{TP}}$. When N_0 varies within a range but the range is smaller, the $M - R$ index will be between the two cases where N_0 is fixed and has a wide range.

4 DISCUSSION

In Section 2, we obtained the column density profiles of 135 clumps in Cygnus-X. Their main features are: 1) the profiles all show broken power-law shapes at $0.1 - 10$ pc, 2) the parameters of each clump's profile are different, 3) the transition points of the profiles are around 0.8 pc and 10^{22} cm^{-2} , suggesting density profiles of $\rho \propto R^{-1.63}$ in the inner part and $\rho \propto R^{-1.11}$ in the outer part. These two parts of density profiles are consistent with the circumstances of free-fall collapse ($\rho \propto R^{-\alpha}$, with $\alpha = 1.5 - 2.0$) and turbulence dominated nature ($\alpha \approx 1.0$), respectively. They are also comparable to the log-normal + power-law N-PDF of Cygnus-X. The N-PDF of Cygnus-X has its power-law index at 2.33 (Xing et al. in preparation), corresponding to a density profile of $\rho \propto R^{-1.86}$. The transitional column density between the log-normal and power-law parts is at $1.86 \times 10^{22} \text{ cm}^{-2}$. These values are slightly different from the parameters of our density profiles, which is because the power-law index of a N-PDF is more affected by the densest sources, and the transitional column density is related to the proportion of high and low density components. These all suggest that the broken power-law column density profiles imply

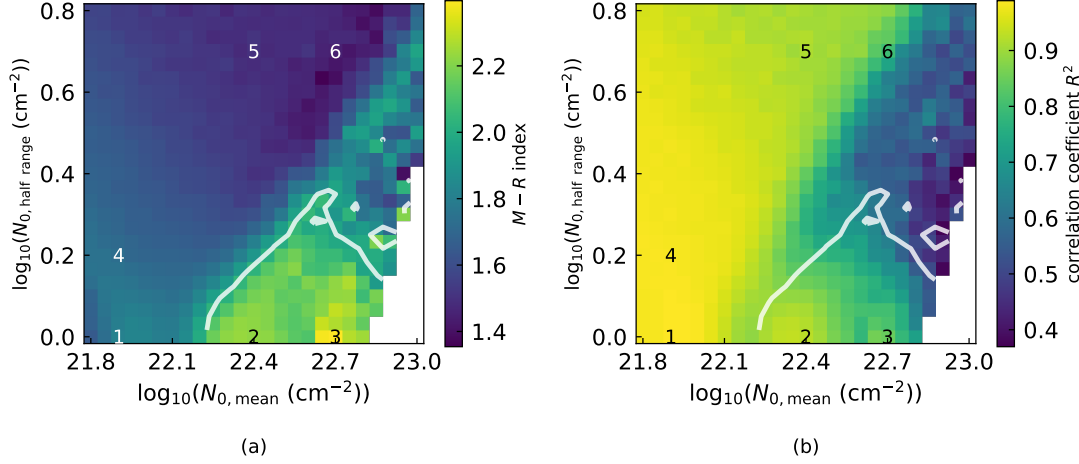


Fig. 9: The $M - R$ indexes (left) and the $M - R$ fitting results' correlation coefficients (right) of the 135 clumps. The column density threshold N_0 is defined by $\log_{10}(N_0) = \log_{10}(N_{0,\text{mean}}) \pm \log_{10}(N_{0,\text{halfrange}})$. The numbers correspond to the cases in Figure 8. White contours show $M - R$ indexes of 2.

a gravity-dominated dense core + turbulence-dominated diffuse cloud, and the transition point at 0.8pc and 10^{22}cm^{-2} acts as the division of the two components.

In Section 3 we show how the $N(R)$ profiles and N_0 affect the shape of the $M - R$ relation. From the observational point of view, N_0 is often determined by the detection limit or set by a threshold in some source extraction method (Kegel 1989; Scalo 1990; Ballesteros-Paredes & Mac Low 2002), and it is likely to be constant. In such a situation the $M - R$ relation may show the well-known $M \propto R^2$ scaling law (Lombardi et al. 2010; Ballesteros-Paredes et al. 2012), provided $N_0 \geq N_{\text{TP}}$ and the power-law index n is nearly constant; the $M - R$ power-law indexes may be slightly less than 2 if N_0 is lower than N_{TP} (Figure 8.1); the $M - R$ relation may also appear to be steeper than $M \propto R^2$, as seen in some other studies (Roman-Duval et al. 2010; Kainulainen et al. 2011), when $N_0 \geq N_{\text{TP}}$ and the power-law index n varies from source to source.

When many molecular cloud structures are included in an analysis (Larson 1981; Urquhart et al. 2014, 2018), N_0 is likely to have a wide distribution, if the cloud structures under investigation were obtained from different observations or extracted from highly varying backgrounds. In these cases, the derived $M - R$ relations may to some extent manifest the density profiles of the cloud structures. But caution should be taken in converting the observed $M - R$ relation to a density profile if the observations significantly suffered from short dynamical ranges (e.g., Scalo 1990; Ballesteros-Paredes & Mac Low 2002; Schneider & Brooks 2004). For molecular cloud structures in Cygnus-X, a $M \propto R^{1.9}$ relation is expected to be obtained with an observational study capable of trimming the structures at large and varying radii (e.g., at $R > 1\text{pc}$ and $N < 10^{22}\text{cm}^{-2}$), as a consequence of a tight distribution of the power-law indexes for the density profiles in the outer parts (i.e., $\rho \propto R^{-1.1}$, see Section 2). Shallower relations can be found at smaller scales and higher densities. They correspond to $\rho \propto R^{-\alpha}$ density distributions with α clearly larger than 1.

Applying different source extraction or identification algorithms to the same molecular cloud, different structures (Schneider & Brooks 2004; Li et al. 2020) and $M - R$ relations (Schneider & Brooks 2004) can be obtained. Without knowing the impact on N_0 of the source extraction process, it is difficult to make convincing interpretations of the $M - R$ relations. For example, $\rho \propto R^{-1}$ profiles and a constant N_0 can both result in $M \propto R^2$ relations. Stronger line-of-sight contamination for larger cloud structures (Ballesteros-Paredes et al. 2019), an approximately constant volume density for all the cloud structures under investigation (Lada et al. 2008; Li & Zhang 2020), and variation from source to source

in the power-law index of the $N(R)$ profiles can all lead to $M - R$ relations steeper than $M \propto R^2$, but only when N_0 is constant or falls in a narrow range can a steep $M - R$ relation come from the difference in the $N(R)$ index. Therefore, before interpreting an $M - R$ relation, one is suggested to carefully check how the cloud structures in the sample are derived and then to determine if a constant N_0 , or instead a varying N_0 , is implicitly being used; only in the latter case, the observed $M - R$ relation could be useful in constraining the averaged density profile of the cloud structures under investigation. From another perspective, an observational experiment optimized for converting a $M - R$ relation to a density profile would require high resolution and high sensitivity to reasonably resolve each source and allow an estimate of the source flux and size free of sensitivity limitation (e.g., estimation based on the peak intensity and FWHM size by 2D Gaussian fitting to the source brightness distribution). This way one equivalently has N_0 varying from source to source. High resolution also helps to minimize potential line-of-sight contamination, while high sensitivity observations of optically thin tracers are desirable to increase the dynamical range.

Can $M - R$ relations help to determine whether the cloud structures are in virial equilibrium? Due to the lack of velocity information, $M - R$ relations cannot be directly linked to the virial state. However, having the linewidth - size relation of $\sigma_v \propto R^{0.5}$ satisfied (Larson 1981; Myers et al. 1983; Solomon et al. 1987; Falgarone et al. 2009), the $M \propto R^2$ relation is suggested to imply that the cloud structures are in virial equilibrium (Larson 1981; Solomon et al. 1987). However, as we discussed above, the $M \propto R^2$ relation does not necessarily mean a density profile of $\rho \propto R^{-1}$, and thus cannot be a straightforward indicator of virial equilibrium. When the $M \propto R^2$ relation is verified to imply $\rho \propto R^{-1}$, and if the structures also follow $\sigma_v \propto R^{0.5}$, the gravitational to kinetic energy ratio is a constant, and means virial equilibrium if that constant is about 2 (Myers & Goodman 1988; Ballesteros-Paredes 2006).

5 SUMMARY

Using the column density map from Cao et al. (2019), we obtain $N(R)$ profiles of 135 dense structures in Cygnus-X. At $0.1 - 10$ pc, all the structures have broken power-law $N(R)$ profiles, suggesting their dense core + diffuse cloud nature. With the transition at approximately 0.8 pc and 10^{22} cm^{-2} , the $N(R)$ profiles have a power-law index of 0.63 ± 0.59 at small radii, and 0.11 ± 0.20 at large radii.

We explore the $M - R$ relation using the broken power-law $N(R)$ profiles. Both the $N(R)$ profiles and the column density threshold N_0 determine the shape of the $M - R$ relation: for $N_0 > N_{\text{TP}}$, we find (1) constant $N(R)$ power-law index and N_0 lead to $M \propto R^2$, (2) the $N(R)$ index with a wide range steepens the $M - R$ relation, (3) N_{TP} and R_{TP} with wider ranges make the data points in the $M - R$ plot spread out along loci following $M \propto R^2$, (4) N_0 with a wide range tend to make the $M - R$ relation follow $M(R)$ profiles. For $N_0 < N_{\text{TP}}$, the fact that n is larger than m makes the $M - R$ index slightly lower than 2. We apply N_0 with different means and ranges to the 135 Cygnus-X clumps and obtain $M - R$ relations with power-law indexes ranging from 1.4 to 2.4.

From the observational perspective, the column density threshold N_0 in extracting cloud structures plays a crucial role in shaping the $M - R$ relation. With a constant N_0 , the $M - R$ relation cannot be a probe of the density profile. Its $M - R$ index can be slightly less than 2 (when $N_0 < N_{\text{TP}}$), equal to 2 (when $N_0 \geq N_{\text{TP}}$ and n has a tight distribution), and larger than 2 (when $N_0 \geq N_{\text{TP}}$ and n has a wide range). For the cases with N_0 having a wide distribution and the data were not significantly affected by line-of-sight contamination or limited by small dynamical ranges, the $M - R$ relation can to large extent be a manifestation of the density profile.

Acknowledgements This work was supported by National Key R&D Program of China No. 2017YFA0402600. We acknowledge the support from National Natural Science Foundation of China (NSFC) through grants U1731237, 11473011, 11590781 and 11629302.

References

Arzoumanian, D., André, P., Didelon, P., et al. 2011, *Astronomy and Astrophysics*, 529, L6 2

- Ballesteros-Paredes, J. 2006, *Monthly Notices of the Royal Astronomical Society*, 372, 443 12
- Ballesteros-Paredes, J., D'Alessio, P., & Hartmann, L. 2012, *Monthly Notices of the Royal Astronomical Society*, 427, 2562 2, 5, 6, 11
- Ballesteros-Paredes, J., Román-Zúñiga, C., Salomé, Q., Zamora-Avilés, M., & Jiménez-Donaire, M. J. 2019, *Monthly Notices of the Royal Astronomical Society*, 490, 2648 11
- Ballesteros-Paredes, J., & Mac Low, M. 2002, *The Astrophysical Journal*, 570, 734 2, 4, 11
- Beaumont, C. N., Goodman, A. A., Alves, J. F., et al. 2012, *Monthly Notices of the Royal Astronomical Society*, 423, 2579 2
- Cao, Y., Qiu, K., Zhang, Q., et al. 2019, *The Astrophysical Journal Supplement Series*, 241, 1 2, 12
- Enoch, M. L., Young, K. E., Glenn, J., et al. 2006, *The Astrophysical Journal*, 638, 293 2
- Falgarone, E., Pety, J., & Hily-Blant, P. 2009, *Astronomy and Astrophysics*, 507, 355 12
- Heyer, M., Krawczyk, C., Duval, J., & Jackson, J. M. 2009, *Astrophysical Journal*, 699, 1092 2
- Kainulainen, J., Beuther, H., Banerjee, R., Federrath, C., & Henning, T. 2011, *Astronomy and Astrophysics*, 530, A64 11
- Kauffmann, J., Pillai, T., Shetty, R., Myers, P. C., & Goodman, A. A. 2010, *Astrophysical Journal*, 712, 1137 2
- Kegel, W. 1989, *Astronomy and astrophysics (Berlin. Print)*, 225, 517 2, 4, 11
- Kellermann, K. I., & Moran, J. M. 2001, *Annual Review of Astronomy and Astrophysics*, 39, 457 1
- Lada, C. J., & Dame, T. M. 2020, *The Astrophysical Journal*, 898, 3 2
- Lada, C. J., Lada, E. A., Clemens, D. P., & Bally, J. 1994, *The Astrophysical Journal*, 429, 694 1
- Lada, C. J., Muench, A. A., Rathborne, J., Alves, J. F., & Lombardi, M. 2008, *The Astrophysical Journal*, 672, 410 11
- Larson, B. 1981, *Monthly Notices of the Royal Astronomical Society*, 194, 809 1, 2, 11, 12
- Li, C., Wang, H.-C., Wu, Y.-W., Ma, Y.-H., & Lin, L.-H. 2020, *Research in Astronomy and Astrophysics*, 20, 031 11
- Li, G.-X., & Zhang, C.-P. 2020, *The Astrophysical Journal*, 897, 89 11
- Lin, Y., Csengeri, T., Wyrowski, F., et al. 2019, *Astronomy and Astrophysics*, 631, A72 2
- Lombardi, M., & Alves, J. 2001, *Astronomy and Astrophysics*, 377, 1023 1
- Lombardi, M., Alves, J., & Lada, C. J. 2010, *Astronomy and Astrophysics*, 519, L7 2, 11
- Mannfors, E., Juvela, M., Bronfman, L., et al. 2021, *Astronomy and Astrophysics*, 654, A123 2
- Massi, F., Weiss, A., Elia, D., et al. 2019, *Astronomy and Astrophysics*, 628, A110 2
- Men'Shchikov, A., André, P., Didelon, P., et al. 2012, *Astronomy and Astrophysics*, 542 2
- Motte, F., Bontemps, S., & Louvet, F. 2018, *Annual Review of Astronomy and Astrophysics*, 56, 41 2
- Motte, F., Bontemps, S., Schilke, P., et al. 2007, *Astronomy and Astrophysics*, 476, 1243 2
- Myers, P. C., & Goodman, A. A. 1988, *ApJ*, 326, L27 12
- Myers, P. C., Linke, R. A., & Benson, P. J. 1983, *The Astrophysical Journal*, 264, 517 12
- Pilbratt, G. L., Riedinger, J. R., Passvogel, T., et al. 2010, *Astronomy and Astrophysics*, 518, L1 2
- Pirogov, L. E. 2009, *Astronomy Reports*, 53, 1127 2
- Pirogov, L., Zinchenko, I., Caselli, P., & Johansson, L. E. 2007, *Astronomy and Astrophysics*, 461, 523 2
- Roman-Duval, J., Jackson, J. M., Heyer, M., Rathborne, J., & Simon, R. 2010, *Astrophysical Journal*, 723, 492 2, 11
- Rygl, K. L. J., Brunthaler, A., Sanna, A., et al. 2012, *Astronomy and Astrophysics*, 539, A79 2
- Scalo, J. 1990, in *Astrophysics and Space Science Library*, Vol. 162, *Physical Processes in Fragmentation and Star Formation*, ed. R. Capuzzo-Dolcetta, C. Chiosi, & A. di Fazio, 151 2, 4, 11
- Schneider, N., & Brooks, K. 2004, *Publications of the Astronomical Society of Australia*, 21, 290 2, 11
- Schneider, N., André, P., Könyves, V., et al. 2013, *The Astrophysical Journal*, 766, L17 2
- Solomon, P. M., Rivolo, A. R., Barrett, J., & Yahil, A. 1987, *The Astrophysical Journal*, 319, 730 12
- Traficante, A., Duarte-Cabral, A., Elia, D., et al. 2018, *Monthly Notices of the Royal Astronomical Society*, 477, 2220 2

- Urquhart, J. S., Moore, T. J., Csengeri, T., et al. 2014, *Monthly Notices of the Royal Astronomical Society*, 443, 1555–11
- Urquhart, J. S., König, C., Giannetti, A., et al. 2018, *Monthly Notices of the Royal Astronomical Society*, 473, 1059–2, 11
- Uyaniker, B., Fürst, E., Reich, W., Aschenbach, B., & Wielebinski, R. 2001, *Astronomy and Astrophysics*, 371, 675–2
- Wang, Y., Qiu, K., Cao, Y., et al. 2022, *The Astrophysical Journal*, 927, 185–2
- Wendker, H. J., Higgs, L. A., & Landecker, T. L. 1991, *Astronomy and Astrophysics*, 241, 551–2